Title

Corrosion inhibition of mild steel by metal cations in high pH simulated fresh water at different temperatures

Author Names

Md. Saiful Islam[1), 2)] Masatoshi Sakairi[3)]

Affiliations

1) Graduate School of Engineering, Hokkaido University, Kita-13, Nishi-8, Kita-ku, Sapporo, Hokkaido 060-8628, Japan.
2) Department of Applied Chemistry & Chemical Engineering, University of Rajshahi, Rajshahi-6205, Bangladesh.
3) Faculty of Engineering, Hokkaido University, Kita-13, Nishi-8, Kita-ku, Sapporo, Hokkaido 060-8628, Japan.

Abstract

Corrosion inhibition effect of metal cations on mild steel was investigated by immersion tests and electrochemical impedance spectroscopy in simulated fresh water with high pH at different temperatures. Immersion tests showed the different corrosion rates in the different solutions, and the Zn^{2+} containing solution showed the minimum corrosion rate at the experimental temperatures. The specimen immersed in the Zn^{2+} containing solution showed comparatively smooth surface which was observed by scanning electron microscopy and atomic force microscopy. EIS and XPS results suggested that Zn^{2+} attached to the steel surface and formed a layer, thereby improving the corrosion inhibition ability of steel.

Keywords: Mild steel; passive films; SEM; XPS; EIS.

1. Introduction

Mild steels are very common and widely used metallic material due to low cost and good mechanical properties. These steels are used in the room temperature and in high temperatures environments such as boilers, liquid transportation pipelines and machinery parts. Corrosion of steel is a serious problem that depends on some important factors such as dissolved oxygen, concentration of Cl^-, pH and temperature of the environment. There are many studies have been carried out on corrosion of mild steel in aqueous environment [1-8]. Passive films on the surface have a great influence on corrosion inhibition of steel, and the stability and structure of the passive films depends on the environmental conditions. The passive films are usually destroyed in presence of anions especially Cl^- [9-12], and after destruction of the passive films, metal dissolution starts with a coupled of electrochemical reactions (cathodic and anodic reactions).

There are several studies have been carried out that metal cations inhibit the corrosion of steel in aqueous solutions [13-26]. Drazic *et al*. [13] explained that Cd^{2+}, Mn^{2+} and Zn^{2+} inhibited the corrosion of iron by lowering the hydrogen evaluation current density in H_2SO_4 solutions at room temperature. Leidheiser Jr. *et al*. [14, 15] explained that some metal cations act as an effective corrosion inhibitors under certain experimental condition. They reported that Sn^{2+} and Pb^{2+} effectively inhibited the corrosion of iron and steel in acid solutions by changing the protective nature of oxide on the surface, and Co^{2+} and Ni^{2+} effectively inhibited the corrosion of galvanized steel in 3% NaCl solutions by forming an insoluble barrier layer at the metal surface. Application of rare earth (RE) metal cation as a corrosion inhibitor was first proposed by Goldie and McCarrol in 1984. Khedr *et al*. [16, 17] reported the effect of some metal cations (K^+, Mg^{2+}, Cu^{2+}, Zn^{2+}, Hg^{2+}, Cd^{2+}, Co^{2+} and Ni^{2+}) on the corrosion of aluminum in neutral and acid Cl^- solutions. In some nuclear power reactors, zinc ions are added into high temperature water for suppressing corrosion of the reactor component materials [18]. Zhang *et*

al. [19] reported that the inhibition effect of metal cations (Na^+, Ca^{2+}, Mn^{2+} and Zn^{2+}) to intergranular stress corrosion cracking of sensitized type-304 stainless steel in 10^{-5} kmol/m^3 sulfate solutions, and they showed that hard metal cation forms a layer on the surface by bonding with the surface film. Amadeh *et al*. [20] introduced the usages of rare earth metal cations (Ce^{4+} and La^{4+}) as corrosion inhibitors for carbon steel in aerated NaCl solution. Otani *et al*. [21] reported that the inhibition effects of metal cations (Na^+, K^+, Ca^{2+}, Mg^{2+}, Zn^{2+} and Ni^{2+}) on corrosion of A3003 aluminum alloy in model tap water at room temperature, and they [22] also reported that Zn^{2+} and Al^{3+} significantly inhibited the corrosion of mild steel in model fresh water. Islam *et al*. [23-25] reported that Zn^{2+} inhibited the corrosion of mild steel in Cl^- aqueous solution at room temperature, and they [26] also explained that Al^{3+} significantly inhibited the corrosion of type-304 stainless steel in 0.5 mol L^{-1} Cl^- aqueous solution at room temperature. Several researchers also reported that metal cations significantly enhanced the inhibition performance of some corrosion inhibitors [27-34]. Therefore, it has been established that metal cations significantly inhibit the corrosion of metal in aqueous solutions.

Almost all of studies regarding the corrosion inhibition of metal by metal cations have been carried out at room temperature, and the inhibition effects were not fully explained as well. Moreover, it is still not fully elucidated the mechanism of corrosion inhibition effect of metal cations on mild steel in fresh water with a high pH at different temperatures. In the case of boiler feed water, the pH is usually controlled at a value of higher than 9.5 [35-38] to avoid the formation of carbonic acid (H_2CO_3) and its species (HCO_3^-) [39]. Therefore, the experimental tests were carried out in fresh water with a high pH (9.5). The present research purpose is to clarify the mechanism of inhibition effects of metal cations on corrosion of mild steel at different temperatures in the high pH simulated fresh water.

In the present study, the differences in the corrosion inhibition abilities of Na^+, Mg^{2+}, Zn^{2+} and Al^{3+} in the high pH simulated fresh water at different temperatures were investigated by

electrochemical impedance spectroscopy (EIS) and immersion tests with mass loss measurement. Influences of metal cations on the surface film structure of mild steel were analyzed by X-ray photoelectron spectroscopy (XPS), and changes in the surface morphology due to immersion in the solutions were observed by scanning electron microscope (SEM) and atomic force microscope (AFM).

2. Experimental

2.1 Specimens

The composition (mass%) of mild steel samples used for this experiment was as follows: C = 0.02; Mn = 0.18; P = 0.015; S < 0.01; and Fe = balance. The mild steel sheet of 0.7 mm thickness was cut into 7 × 7 mm to carried out different tests. For the potentiodynamic polarization and EIS measurements, each specimen was connected to a conductive wire and embedded in epoxy resin leaving the exposed surface. For the immersion corrosion tests, the specimens were also embedded in resin leaving the exposed surface. For both experiments, the exposed surface of specimens was mechanically abraded with a series of SiC abrasive paper up to #4000 grit size. In the case of immersion tests, the abraded specimens were removed from the resin beforehand the tests. Before the experimental tests, all the specimens were ultrasonically cleaned in ethanol and in highly purified water.

2.2 Test solutions

Three different salt solutions of 10^{-4} mol L^{-1} $MgCl_2$ (Mg_{sol}), 10^{-4} mol L^{-1} $ZnCl_2$ (Zn_{sol}) and 10^{-4} mol L^{-1} $AlCl_3$ (Al_{sol}) were prepared. The Cl^- concentration also plays an important role in corrosion of metals, therefore, the concentration of Cl^- of all these solutions was adjusted to 10^{-3} mol L^{-1} by NaCl, which is similar to that of usual fresh water [22]. These solutions were used as test solutions together with 10^{-3} mol L^{-1} NaCl (Na_{sol}) which was used as a reference

solution. The pH of the solutions was adjusted to about 9.5 using 10^{-1} mol L^{-1} NaOH (Table 1). Fig. S1 shows the condition of solutions before the experiment.

The pH of the solutions before and after immersion tests was measured by the pH meter (Eutech Instruments, Cyber-Scan 6000). Water used in this experiment was highly purified (MILLIPORE, Simplicity UV). Before the experiment, all the test solutions were colorless and transparent (Fig. S1). All the chemicals used in this study were commercially available special grade and were obtained from Kanto Chemical Co. Ltd.

2.3 Immersion tests

Specimens were immersed in each solution at 25, 50 and 80°C for 1, 2 and 3 d. Immersion tests were carried out with three replicates of each solution in each temperature at a time. The exposed surface area of the specimens was 0.49 cm^2, and the test was carried out by keeping the solutions open to the air. The mass of the specimen before and after the tests was measured using a microbalance (METTLER TOLEDO MX5, Pro FACT) to obtain the mass change. Corrosion rates and the corrosion inhibition efficiencies of metal cations were calculated based on the mass loss during the immersion tests by the Eqs. (1) and (2) [23-26].

$$\text{Corrosion rate } (\mu m/y) = \frac{M_1 - M_2}{D \times S \times t} \times 365 \times 10000 \quad (1)$$

Here M_1 (g) is the mass of the specimen before immersion, M_2 (g) is the mass of the specimen after immersion, D (g/cm^3) is the density of the specimen, S (cm^2) is the surface area of the specimen and t (d) is the immersion time.

$$\text{Corrosion inhibition efficiency } (\%) = \frac{Na_{CR} - CAT_{CR}}{Na_{CR}} \times 100 \quad (2)$$

Here Na_{CR} is the corrosion rate of specimens immersed in the Na_{sol}, and CAT_{CR} is the corrosion rate of specimens immersed in Mg_{sol}, Zn_{sol} and Al_{sol}, and the corrosion inhibition efficiency of Na^+ is considered zero.

A digital camera (Nikon, D80) was used for taking the photograph of the sample surface and the glass container overview before and after immersion, a scanning electron microscope (SEM, JEOL, JSL6510-LA) was used for high magnification observation of the sample surface. The red color corrosion products (rust) formed on the specimen surface after immersion in the solutions was analyzed by X-ray diffraction (XRD, Rigaku, SmartLab). For the processing of XRD data, integrated X-ray powder diffraction software (PDXL2) was used. The surface roughness [40, 41] was measured by atomic force microscope (AFM, SPA400) using dynamic force mode with the cantilever type, SI-DF40. X-ray photoelectron spectroscope (XPS, JEOL, JPS-9200) was used for surface analysis. During the XPS analysis, Al Kα was used as an X-ray source (1486.6 eV), and the measurement region of photoelectrons was 3×3 mm. The XPS depth analysis was carried out by sputtering of Ar ion. The sputtering time was converted to depth by the sputtering rate of SiO_2. Before the surface observation and analysis, the immersed specimens were cleaned ultrasonically first in ethanol and then in highly purified water.

2.4 Electrochemical measurements

Electrochemical tests were performed in a conventional three-electrode cell using a potentiostat (IVIUM TECHNOLOGIES, Pocketstat) connected to a personal computer. The tests were carried out with three replicates of each solution at 25, 50 and 80°C. Before the tests, the specimens were immersed in the solutions for 1 h at all these temperatures. A Pt plate was used as the counter electrode and the reference electrode was Ag(s)|AgCl(s)|Cl^- (aqueous, saturated KCl) (SSE). The exposed surface area of the specimen (working electrode) in the solution was 0.49 cm^2. The polarization measurements were carried out from immersion potential to the cathodic and anodic direction with a scan rate of 60 mV/min. The cathodic and anodic scan was started individually to obtain the specific electrochemical properties of mild steel immersed in the solutions with metal cations. The EIS measurements were carried out at

open circuit potential in the frequency range from 10 kHz to 1 mHz and a modulation amplitude of 10 mV. The IVIUM software was used to fit the EIS data.

3. Results and discussions

3.1 Immersion tests

The appearances of solutions and specimens after immersion in the solutions for 1, 2 and 3 d at 25, 50 and 80°C are shown in Fig. S2. The brightness of the solutions is different and the Zn_{sol} is brighter as compared to the other solutions after 3 d immersion at 80°C. Red color corrosion products are observed on the specimens and in the solutions. The appearances (red color) and the brightness of the solutions may indicate the degree of corrosion of steel in the solutions. Fig. S3 a) and b) show the appearances of the specimen surfaces after immersion in the solutions for 3 d at 25, 50 and 80°C before the ultrasonic cleaning and after the ultrasonic cleaning respectively. All the cases red corrosion products (rust) are found on the specimen surface (Fig. S3 a)).

The pH of the test solutions before and after immersion for 3 d at 25, 50 and 80°C are shown in Table 1, where pH_{int} is the initial pH of solutions, pH_{corr} is the pH obtained after immersion tests. The pH is decreased after immersion (pH_{corr}) in all solutions of metal cations. Several researchers also reported that the pH of solutions in such cases decreases with the hydrolysis of Fe^{2+} and Fe^{3+} [42, 43].

The mass of specimens was measured after immersion in the solutions at 25, 50 and 80°C for 1, 2 and 3 d. Fig. 1 a) shows the average mass changes of specimens with time. After 1 d immersion in the solutions, it is found that the average mass changes of specimens immersed in Mg_{sol}, Zn_{sol}, and Al_{sol} are nearly the same, whereas the average mass change of the specimen immersed in Na_{sol} is different. The average mass changes of specimen are gradually increasing with time. After 2 and 3 d immersion, each solution shows the different mass change, and Na_{sol}

shows the highest mass change and Zn_{sol} shows the lowest mass change as compared to the other solutions at all of the experimental temperatures.

The corrosion rates were calculated from the mass change after immersion in the solutions at 25, 50 and 80°C for 3 d. Fig. 1 b) shows the corrosion rates at different temperatures. The corrosion rate is gradually increasing with increasing the temperature. Na_{sol} shows the highest and Zn_{sol} shows the lowest corrosion rate as compared to the other solutions at all these temperatures. This result indicates that Zn_{sol} has better corrosion inhibition ability than other solutions.

3.2 Surface observations and analysis

Corrosion behavior of specimens can be clarified by surface morphology changes that are occurred due to immersion in the solutions. The surface morphologies were observed by SEM to clarify the situation. Fig. 2 shows the surface SEM images of specimen immersed in the solutions at 25, 50, and 80°C for 1, 2 and 3 d. Different surface morphologies are observed on the specimen immersed in the different solutions. SEM images clearly indicate the numbers of pits and grain boundaries that are observed on the surface of specimen immersed in Na_{sol}, Mg_{sol} and Al_{sol} at all the temperatures. The clearer grain boundaries are observed with increasing the temperatures on the surface of specimen immersed in Na_{sol}, Mg_{sol} and Al_{sol}. These clear grain boundaries and pits represent the severe corrosion occurred on the mild steel surface. Some small pits are observed on the surface of specimen immersed in Zn_{sol}, and the numbers of pits are increased with increasing the temperatures. Relatively smooth surface is observed on the specimen immersed in Zn_{sol} as compared to the others. The results of surface observations are in good agreement with the corrosion rate as showed in the Fig. 1 b).

The surface roughness of each specimen was measured by AFM after immersed in the solutions at 25, 50, and 80°C for 3 d, and the AFM-3D images are shown in the Fig. S4. Different surface roughness is observed of specimen immersed in the different solutions with

metal cations. The average surface roughness (R_a) was calculated from the respective 3D images to enumerate the surface roughness. The calculated R_a values are shown in Fig. 3 as a function of temperature. For all the cases, average surface roughness is increased with increasing the temperature. However, the specimen immersed in the Zn_{sol} shows the lowest R_a as compared to the specimen immersed in the other solutions. Zn related products may be covered the steel surface and thus metal dissolution reactions were inhibited. From this reason specimen immersed in the Zn_{sol} showed the lowest roughness. These results correspond well to the surface observation by SEM as showed in the Fig. 2.

The red corrosion products (rust) formed on the specimen surface shown in Fig. S3 a) were analyzed by XRD to determine the crystal structure. Fig. 4 shows XRD patterns of the corrosion products on specimens after immersion in the solution at 80°C for 3 d. The results indicate that the corrosion products formed on the specimen surface in all the solutions consisted of FeOOH, Fe_3O_4, Fe_2O_3, and Fe, and metal cations are not detected in the corrosion products.

The specimen surfaces were examined by XPS to clarify the existence of metal cations on the mild steel surface after immersion in the solutions. Fig. 5 shows the results of XPS analysis of the surface of specimen immersed in each solution at 25, 50, and 80°C for 1 h. In the wide spectra, Zn2p1/2 and Zn2p3/2 peaks are observed on the specimens immersed in the solution at all temperatures whereas the other peaks of Na1s, Mg1s, and Al2p3/2 are not observed on the specimen immersed in the corresponding solution. This result indicates that only Zn existed on the surface after immersion in the Zn_{sol} at all the experimental temperatures. XPS narrow scan with depth was performed to determine how Zn was distributed in the surface films. Right side of Fig. 5 shows the XPS narrow spectra of Zn2p3/2 with depth at 25, 50 and 80°C. At 25°C, sharp peaks of Zn2p3/2 are appeared with a depth of approximately 100 nm. It means that the thickness of the Zn-layer is about 100 nm. At 50 and 80°C, peaks of Zn2p3/2 are also appeared and the thickness of the layers are approximately 20 nm and 10 nm respectively. The

results suggest that Zn-layer exists on the surface at all temperatures. However, the thickness of the Zn-layer is decreased with increasing the temperature.

XPS narrow scan was analyzed to determine the chemical state of zinc that is existed on the steel surface. Fig. 6 shows the XPS narrow scan of Zn2p3/2 at 25, 50, and 80°C. In the case of 25°C (Fig. 6 a)), the peak of Zn2p3/2 is observed at 1022.5 eV (binding energy) which is related to the peak of Zn^{2+} and it is indicated to the formation of zinc hydroxide ($Zn(OH)_2$) [44, 45]. Leygraf *et al*. [46] and Winiarski *et al*. [47] reported about the formation of corrosion product of Zn^{2+} as zinc hydroxide ($Zn(OH)_2$) and carbonate based corrosion product as hydrozincite ($Zn_5(CO_3)_2(OH)_6$) on the steel surface at normal temperature. In the case of 50°C and 80°C (Fig. 6 b) and c)), the peak of Zn2p3/2 is observed at 1021.4 eV (binding energy) which is also related to the peak of Zn^{2+} and it is indicated to the formation of zinc oxide (ZnO) [44, 45]. Zhang [48] reported that $Zn(OH)_2$ is generally the corrosion product formed in zinc containing water in the temperature range 0-30°C, and ZnO is the corrosion product in the temperature range 30-90°C. Winiarski *et al*. [47] also reported that ZnO is formed at the temperature around 60°C. Therefore, from the XPS results, it can be suggested that Zn^{2+} existed on the specimen surface as zinc hydroxide ($Zn(OH)_2$) and carbonate based zinc corrosion product as hydrozincite ($Zn_5(CO_3)_2(OH)_6$) at 25°C, and at the higher temperatures (50°C and 80°C) Zn^{2+} existed on the specimen surface as zinc oxide (ZnO) after immersion in the solution, and it further made a chemical bond with the passive films which led to a layer of Zn^{2+}. The layers of Zn^{2+} may have protected the steel from the Cl^- attack and inhibited the metal dissolution reactions. The Zn-layer may have also some defects, and the area of defect may be increased with increasing the temperature. The defects of film further led to the formation of pits [34] and the numbers of pits were increased with increasing the temperatures which were showed in the Fig. 2. From this reason, the metal dissolution rate in Zn_{sol} (Fig. 1 b)) also increased with increasing the temperature. Na^+ cannot existed on the steel surface as oxides or

hydroxides in the experimental conditions [22-26, 49]. From the mass change after 1 d immersion in the solutions (Fig. 1 a)), it is signifying that Mg^{2+} and Al^{3+} may be precipitated as oxides or hydroxides on the steel surface which inhibited the metal dissolution like as Zn^{2+}. However, the precipitations of both Mg^{2+} and Al^{3+} might not be stable and cannot form bond with the surface film with time as larger mass changes were observed compared with Zn_{sol} after 2 and 3 d immersion (Fig. 1 a)). From these reasons the corrosion rate in Mg_{sol} and Al_{sol} showed lower than that in Na_{sol} and higher than that in Zn_{sol}, and the lowest corrosion rate was observed in Zn_{sol} as compared to the other solutions (Fig. 1 b)) at the experimental temperatures.

3.3 Electrochemical tests

3.3.1 Polarization curves

From the immersion tests results (surface observations and analysis), Zn_{sol} showed better corrosion inhibition ability than other solutions. Therefore, the polarization behavior was studied only in Na_{sol} and Zn_{sol} at 25, 50 and 80°C. The potentiodynamic polarization curves are shown in Fig. 7. Fig. 7 a) shows the cathodic polarization curves in Na_{sol} and Zn_{sol} at 25, 50 and 80°C. At 25°C, higher current density is observed in Na_{sol} than that in Zn_{sol} at around the potential -0.5 V, and after the potential at around -1.0 V, there is no significant difference in the current density between Na_{sol} and Zn_{sol}. At 50°C, higher current density is observed in Zn_{sol} than that in Na_{sol} at around the potential -0.5 V. However, after the potential at -1.0 V, Zn_{sol} shows lower current density than that in Na_{sol}. At 80°C, Na_{sol} shows higher current density than that in Zn_{sol} after the potential at around -1.0 V. Fig. 7 b) shows the anodic polarization curves in Na_{sol} and Zn_{sol} at 25, 50 and 80°C. Lower current density is observed in Zn_{sol} than that in Na_{sol} at all the experimental temperatures. Therefore, it can be suggested that Zn^{2+} containing solution has inhibition ability both in cathodic and anodic reactions as compared to the Na^{+} containing solution at all the experimental temperatures.

3.3.2 EIS tests

EIS tests were carried out at 25, 50 and 80°C, and Figs. 8 a) to f) show the Bode diagram of impedance and phase shift plots. Fig. 8 g) shows the equivalent circuit which was used to fit the experimental data that simulates an electrode with a protective film having defect [34, 50]. The fitted lines are also shown in Figs. 8 a) to f) which were calculated by the equivalent circuit (Fig. 8 g)). The equivalent circuit consists (Fig. 8 g)) of bulk solution resistance (R_{sol}), resistance of the defects in the protective film (R_d), charge transfer resistance at the metal/solution interface inside the defect (R_{ct}), constant phase element of the double layer at the defect interface (Q_{dl}) and the constant phase element of the protective film (Q_f). The fitted lines correspond well to the experimental plots (Figs. 8 a) to f)). Some pits were also observed on the specimen immersed in the Zn^{2+} containing solutions (as shown in Fig. 2) suggesting that the protective Zn-layer formed on the immersed specimens had some defects that led to the formation of pits [34]. The number of pits on the specimen immersed in the Zn^{2+} containing solution were increased with increasing the temperature (as showed in Fig. 2). The magnitude of impedance indicates the corrosion resistance of steel in the solutions [22-24]. From Fig. 8 a) to f), it is found that the impedance and phase shift are decreased with increasing the temperature. However, Zn_{sol} shows the highest impedance and highest phase shift as compared to the other solutions at all the experimental temperatures. These results indicate that Zn_{sol} has better corrosion resistance ability than the other solutions at the experimental temperatures.

Calculated electrochemical impedance parameters of mild steel after immersion in the solutions for 1 h at different temperatures are shown in Table 2. The corrosion resistance (R_c) and the inhibition efficiency (η) were calculated by the Eqs. (3) and (4):

$$R_c = R_d + R_{ct} \quad (3)$$

$$\eta\% = (R_{c\_sol} - R_{c\_ref})/R_{c\_sol} \times 100 \quad (4)$$

Where R_{c_sol} and R_{c_ref} are the values of corrosion resistance in the solutions (Mg_{sol}, Zn_{sol} and Al_{sol}), and in the reference solution (Na_{sol}). From Table 2, the η and R_c of Zn_{sol} show the

highest value as compared to the other solutions at all the experimental temperatures. These results indicate that the charge transfer may be inhibited by the Zn-layer (in the Zn^{2+} containing solution) that was formed on the steel surface and the inhibition ability was decreased with increasing the temperature. The value of Q_{dl} in Zn^{2+} containing solution (Zn_{sol}) is lower than that in other solutions at all the temperatures. The decrease in Q_{dl} value indicates that the defect in the film is decreased on the mild steel [34, 51]. The results obtained from the EIS tests are in good agreement with the immersion tests results.

3.4 Corrosion inhibition efficiency

From the experimental results, it was found that the solutions containing different metal cations showed different corrosion rate. Therefore, it is considered that Zn^{2+} and Al^{3+} significantly inhibited the metal dissolution in the solutions, and Zn^{2+} containing solution showed the lowest corrosion rate at all the experimental temperatures (as shown in Fig. 1 b)) as compared to the other solutions. The corrosion inhibition efficiencies of metal cations were calculated based on the immersion tests and the Fig. 9 shows the corrosion inhibition efficiencies of metal cations as a function of temperature in which mean values of mass loss data were used. Different corrosion inhibition efficiencies of metal cations are observed at different temperatures. Corrosion rate is increased with increasing the temperature (as shown in Fig. 1 b)), however, corrosion inhibition efficiencies of metal cations are increased at a higher temperature (80°C). Because at a higher temperature corrosion is rapidly increased in Na_{sol} as compared in the other solutions, and efficiencies were calculated by comparing the Na_{sol}. Therefore, Zn^{2+} and Al^{3+} show higher corrosion inhibition efficiency at 80°C, and Zn^{2+} shows the highest corrosion inhibition efficiency as compared to the other metal cations at all the experimental temperatures.

3.5 Corrosion inhibition mechanism

From the above experimental results, Zn^{2+} effectively inhibited the mild steel corrosion in model fresh water as compared to the other metal cations used in this study at the experimental temperatures. Based on the experimental results, a possible corrosion inhibition mechanism of mild steel by Zn^{2+} can be proposed. Fig. 10 shows the Zn^{2+} layer formation on the specimen surface at different temperatures and corrosion inhibition mechanism in the solution. At 25°C, Zn^{2+} layer is formed on the steel surface (Fig. 10 a) and b)). However, Zn^{2+} layer may not cover all the exposed surface of steel, and the layer contains some defects. The Cl^- attack at the defects and initiate the metal dissolution (Fig. 10 b)). When the temperature is increased to 50°C, the thickness of the Zn^{2+} layer is decreased and the area of the defects is increased (Fig. 10 c)). The possible reasons by which the thickness of Zn-layer decreased and the area of the defects increased are as follows:

a) The composition of Zn-layer is changed with temperature as discussed in 'surface observations and analysis.' At 25°C, $Zn(OH)_2$ and $Zn_5(CO_3)_2(OH)_6$ are formed, and at 50 and 80°C, ZnO is formed [44-48]. Thus, the layer thickness is decreased at a higher temperature.

b) Dissolution rate in the layer may increase with increasing the temperature.

c) Some part of the layer may be removed while metal dissolution occurs, and the area of defects increased at a higher temperature.

Due to the above-mentioned reasons, the corrosion rate is increased at a higher temperature as compared to that at a lower temperature. When the temperature is further increased to 80°C, the thickness of the Zn^{2+} layer is decreased and the area of the defects is also increased (Fig. 10 d)). From these points of view, the corrosion rate is increased at 80°C as compared to at 25 and 50°C. However, Zn^{2+} containing solution showed the lowest corrosion rate as compared to

the other solutions at all the experimental temperatures due to inhibition of the corrosion reactions by the Zn^{2+} layer that was formed on the steel surface.

4. Conclusions

The effects of metal cations on the corrosion inhibition of mild steel in simulated fresh water at 25, 50 and 80°C were investigated by immersion tests, EIS tests and surface investigations were carried out by SEM, AFM, and XPS. It can be concluded as follows:

1) The corrosion rate of steel in each solution obtained from the immersion corrosion tests decreased in the order of $Na_{sol} > Mg_{sol} > Al_{sol} > Zn_{sol}$.

2) Comparatively smooth surfaces of the specimens immersed in the Zn_{sol} at all the experimental temperatures were observed by SEM and AFM.

3) The charge transfer resistance (R_{ct}) from the EIS tests decreased in the order of $Zn_{sol} > Al_{sol} > Mg_{sol} > Na_{sol}$. From these, it was suggested that Zn^{2+} present in the aqueous solution had a function of suppressing corrosion.

4) From the XPS analysis of the sample surface immersed in different solutions, only Zn^{2+} was detected on the specimen immersed in the Zn_{sol}.

5) Zn^{2+} formed a layer on the surface films and protected the steel surface from Cl^- attack and inhibited the corrosion reactions.

Acknowledgements

This study was supported by the Japan Boiler Association. SEM observation of this work was conducted at the Laboratory of XPS analysis, Joint-use facilities, Hokkaido University, supported by “Material Analysis and Structure Analysis Open Unit (MASAOU). XPS analysis was conducted at the Laboratory of XPS analysis, Hokkaido University, supported by ‘Nanotechnology Platform’ Program of the Ministry of Education, Culture, Sports, Science and Technology (MEXT), Japan.

References

[1] C. P. Gardiner and R. E. Melchers, Corrosion of mild steel by coal and iron ore, Corros. Sci., 44 (2002) 2665-2673.

[2] R. E. Melchers, Modelling immersion corrosion of structural steels in natural fresh and brackish waters, Corros. Sci., 48 (2006) 4174-4201.

[3] G. A. Rassoul and D. R. Rzaige, Effect of temperature on corrosion of carbon steel boiler tubes in dilute sodium chloride solution, Iraqi J. Chem. Petroleum Eng., 9 (2007) 37-41.

[4] A. C. Uzorh, Corrosion properties of plain carbon steels, IJES, 2 (2013) 18-24.

[5] H. Xian-jun, Z. Bi-ming, C. Shao-hui, F. Feng and J. Jian-qing, Oxide scale growth on high carbon steel at high temperatures, J. Iron Steel Res. Int., 20 (2013) 47-52.

[6] G. S. Vasyliev, The influence of flow rate on corrosion of mild steel in hot tap water, Corros. Sci., 98 (2015) 33-39.

[7] S. Cao, D. Liu, P. Zhang, L. Yang, P. Yang, H. Lu and J. Gui, Green bronsted acid ionic liquids as novel corrosion inhibitors for carbon steel in acidic medium, Scientific Reports, 7 (2017).

[8] X. Zheng, M. Gong, Q. Li and L. Guo, Corrosion inhibition of mild steel in sulfuric acid solution by loquat (Eriobotrya japonica Lindl.) leaves extract, Scientific reports, 8 (2018).

[9] R. T. Foley, Role of the chloride ion in iron corrosion, Corros., 26 (1970) 58-70.

[10] D. D. Macdonald, The point defect model for the passive state, J. Electrochem. Soc., 139 (1992) 3434-3449.

[11] E. McCafferty, Introduction to Corrosion Science, Springer, (2010) 283-286.

[12] Y. Song, G. Jiang, Y. Chen, P. Zhao and Y. Tian, Effects of chloride ions on corrosion of ductile iron and carbon steel in soil environments, Scientific Reports, 7 (2017).

[13] D. M. Drazic and L. Z. Vorkapic, Inhibitory effects of manganeous, cadmium and zinc ions on hydrogen evolution reaction and corrosion of iron in sulphuric acid solutions, Corros. Sci., 18 (1978) 907-910.

[14] H. Leidheiser Jr., A review of proposed mechanisms for corrosion inhibition and passivation by metallic cations, Corros., 36 (1980) 339-345.

[15] H. Leidheiser Jr. and I. Suzuki, Cobalt and nickel cations as corrosion inhibitors for galvanized steel, J. Electrochem. Soc., 128 (1981) 242-249.

[16] M. G. A. Khedr and A. M. S. Lashien, Corrosion behavior of aluminum in the presence of accelerating metal cations and inhibition, J. Electrochem. Soc., 136 (1989) 968-972.

[17] M. G. A. Khedr and A. M. S. Lashien, The role of metal cations in the corrosion and corrosion inhibition of aluminium in aqueous solutions, Corros. Sci., 33 (1992) 137-151.

[18] J. N. Esposito, G. Economy, W. A. Byers, J. B. Esposito, F. W. Pement, R. J. Jacko, C. A. Bergmann, in: Proc. 5th Int. Sympo. Environmental degradation of materials in nuclear power systems-water reactors, American Nuclear Society, (1992) 495-503.

[19] S. Zhang, T. Shibata, T. Haruna, Inhibition effect of metal cations to intergranular stress corrosion cracking of sensitized type 304 stainless steel, Corros. Sci., 47 (2005) 1049-1061.

[20] A. Amadeh, S. R. Allahkaram and S. R. Hosseini, The use of rare earth cations as corrosion inhibitors for carbon steel in aerated NaCl solution, Anti-Corrosion Methods and Materials, 55 (2008) 135-143.

[21] K. Otani, M. Sakairi, R. Sasaki, A. Kaneko, Y. Seki and D. Nagasawa, Effects of metal cations on corrosion behavior and surface film structure of the A3003 aluminum alloy in model tap waters, J. Solid State Electrochem., 18 (2014) 325-332.

[22] K. Otani, M. Sakairi, Effects of metal cations on corrosion of mild steel in model fresh water, Corros. Sci., 111 (2016) 302-312.

[23] Md. S. Islam, K. Otani and M. Sakairi, Effects of metal cations on mild steel corrosion in 10 mM Cl^- aqueous solution, Corros. Sci., 131 (2018) 17-27.

[24] Md. S. Islam, K. Otani and M. Sakairi, Role of metal cations on corrosion of coated steel substrate in model aqueous layer, ISIJ International, 58 (2018) 1616-1622.

[25] Md. S. Islam and M. Sakairi, Effects of Zn^{2+} concentration on the corrosion of mild steel in NaCl aqueous solutions, J. Electrochem. Soci., 166 (2019) C83-C90.

[26] Md. S. Islam, K. Otani and M. Sakairi, Corrosion inhibition effects of metal cations on SUS304 in 0.5 M Cl^- aqueous solution, Corros. Sci., 140 (2018) 8-17.

[27] I. Singh and M. Singh, Effect of metallic cations on the corrosion and the hydrogen absorption by cold-rolled mild steel in inhibited sulfuric acid, Corros., 43 (1987) 425-429.

[28] I. Felhosi, Zs. Keresztes, F. H. Karman, M. Mohai, I. Bertoti and E. Kalman, Effects of bivalent cations on corrosion inhibition of steel by 1-hydroxyethane-1, 1-diphosphonic acid, J. Electrochem. Soc., 146 (1999) 961-969.

[29] J. C. Lin, S. L. Chang and S. L. Lee, Corrosion inhibition of steel by thiourea and cations under incomplete cathodic protection in a 3.5% NaCl solution and seawater, J. App. Electrochem., 29 (1999) 911-918.

[30] J. Telegdi, M. M. Shaglouf, A. Shaban, F. H. Karman, I. Betroti, M. Mohai and E. Kalman, Influence of cations on the corrosion inhibition efficiency of aminophosphonic acid, Electrochim. Acta. 46 (2001) 3791-3799.

[31] M. Abdallah and M. M. El-Naggar, Cu^{2+} cation + 3,5-dimethyl pyrazole mixture as a corrosion inhibitor for carbon steel in sulfuric acid solution, Mater. Chem. Phys., 71 (2001) 291-298.

[32] S. Sathiyanarayanan, C. Jeyaprabha, S. Muralidharan and G. Venkatachari, Inhibition of iron corrosion in 0.5 M sulphuric acid by metal cations, App. Surf. Sci., 252 (2006) 8107-8112.

[33] M. Prabakaran, M. Venkatesh, S. Ramesh and V. Periasamy, Corrosion inhibition behavior of propyl phosphonic acid-Zn^{2+} system for carbon steel in aqueous solution, App. Surf. Sci., 276 (2013) 592-603.

[34] K. Otani, Md. S. Islam and M. Sakairi, Inhibition ability of gluconates for fresh water corrosion of mild steel enhanced by metal cations, *J. Electrochem. Soci.*, 164 (2017) C498-C504.

[35] L. I. Pincus, Practical boiler water treatment-introducing air-conditioning system, McGraw-Hill Book Company, New York, (1962) 37-38.

[36] S. Basu, Boiler chemistry control and treatment of feed water, Elsevier SciTech Connect, (2015).

[37] Handbook of Industrial Water Treatment, General Electric Company, (2012).

[38] E. J. Bonner, Water treatment for modern boiler plant in the paper industry, Prime Conference Proc. Instn. Mech. Engrs., (1967) 24-33.

[39] I. G. Wenten, Khoiruddin, F. Arfianto and Zudiharto, Bench scale eletrodeionization for high pressure boiler feed water, Desalination 314 (2013) 109-114.

[40] A. K. Satapathy, G. Gunasekaran, S. C. Sahoo, K. Amit and P. V. Rodrigues, Corrosion inhibition by justicia gendarussa plant extract in hydrochloric acid solution, Corros. Sci., 51 (2009) 2848-2856.

[41] R. R. L. De Oliveira, D. A. C. Albuquerque, T. G. S. Cruz, F. M. Yamaji and F. L. Leite, Measurement of the nanoscale roughness by atomic force microscopy: Basic principles and applications, Federal University of São Carlos, Campus Sorocaba, Brazil, (2011).

[42] L. N. Mulay and P. W. Selwood, Hydrolysis of Fe^{3+}: magnetic and spectrophotometric studies on ferric perchlorate solutions, J. Am. Chem. Soc., 77 (1955) 2693-2701.

[43] F. H. Sweeton and C. F. Baes Jr., The solubility of magnetite and hydrolysis of ferrous ion in aqueous solutions at elevated temperatures, J. Chem. Thermodynamics, 2 (1970) 479-500.

[44] R. Al-Gaashani, S. Radiman, A. R. Daud, N. Tabet and Y. Al-Douri, XPS and optical studies of different morphologies of ZnO nanostructures prepared by microwave methods, Ceramics Int., 39 (2013) 2283-2292.

[45] N. Gogurla, A. K. Sinha, S. Santra, S. Manna and S. K. Ray, Multifunctional Au-ZnO Plasmonic Nanostructures for Enhanced UV Photodetector and Room Temperature NO Sensing Devices, Scientific Reports, 4 (2014).

[46] C. Leygraf and T. Graedel, Atmospheric Corrosion, *Wiley Interscience*, 131 (2001).

[47] J. Winiarski, W. Tylus, K. Winiarska, I. Szczygiel and B. Szczygiel, XPS and FT-IR characterization of selected synthetic corrosion products of zinc expected in neutral environment containing chloride ions, *J. Spectroscopy*, (2018) 1-14.

[48] X. G. Zhang, Corrosion and Electrochemistry of Zinc, Springer, Boston, MA, (1996).

[49] M. Pourbaix, Atlas of electrochemical equilibria in aqueous solutions, National Association of Corrosion Engineers, Huston, Texas (1974).

[50] F. Vacandio, Y. Massiani, P. Gergaud and O. Thomas, Stress porosity measurements and corrosion behavior of AIN films deposited on steel substrates, Corros. Sci., 359 (2000) 221-227.

[51] M. Mahdavian and R. Naderi, Corrosion inhibition of mild steel in sodium chloride solution by some zinc complexes, Corros. Sci., 53 (2011) 1194-1200.

Captions of Figures and Tables

Table 1 pH of solutions before and after the immersion tests for 3 d at 25, 50 and 80℃.

Table 2 Calculated electrochemical impedance parameters of mild steel after immersion in the solutions for 1 h at different temperatures.

Fig. 1 a) Mass changes of specimens with immersion time and b) Corrosion rate at different temperatures.

Fig. 2 Surface SEM images of specimen after immersion in the solutions for 3 d at 25, 50 and 80°C.

Fig. 3 Average surface roughness of specimens as a function of temperature after immersion in the solutions for 3 d.

Fig. 4 XRD patterns of the corrosion products (rust) formed on specimens after immersion in the solutions for 3 d at 80°C.

Fig. 5 XPS wide spectra of specimen surface after immersion in the solutions for 1 h, and narrow spectra of Zn2p3/2 with depths (inset) at 25, 50 and 80°C.

Fig. 6 XPS narrow spectra of Zn2p3/2 with chemical state and binding energy of specimen surface after immersion in the solutions for 1 h at a) 25°C, b) 50°C and c) 80°C.

Fig. 7 Potentiodynamic a) cathodic and b) anodic polarization curves after immersion in the Na_{sol} and Zn_{sol} for 1 h at 25, 50 and 80°C.

Fig. 8 Bode diagram of impedance and phase shift plots a) and d) at 25°C, b) and e) at 50°C, c) and f) at 80°C, and g) Schematic representation of the equivalent circuit of mild steel electrode with a protective film having a defect.

Fig. 9 Corrosion inhibition efficiency of metal cations as a function of temperature.

Fig. 10 Corrosion inhibition mechanism of mild steel by the Zn-layer at different temperatures, a) Formation of Zn-layer on the steel surface, b) Cl^- attack at the defect sites and initiation of metal dissolution at 25°C, c) decreasing of Zn-layer thickness and increasing of defect area at 50°C, d) decreasing of Zn-layer thickness and increasing of defect area at 80°C.

Table 1 pH of solutions before and after the immersion tests for 3 d at 25, 50 and 80℃.

Solution of metal cations	pH_{int}	pH_{corr}		
		25°C	50°C	80°C
Na_{sol}	9.65	6.45	6.66	6.48
Mg_{sol}	9.60	6.72	6.82	6.52
Zn_{sol}	9.64	6.52	6.95	6.66
Al_{sol}	9.54	6.66	7.04	6.55

Table 2 Calculated electrochemical impedance parameters of mild steel after immersion in the solutions for 1 h at different temperatures.

Solutions	R_c ($k\Omega cm^2$)			Q_{dl} ($\mu s^n \Omega^{-1} cm^{-1}$)			n_{dl}			η (%)		
	25° C	50° C	80° C	25°C	50° C	80°C	25° C	50° C	80° C	25° C	50° C	80° C
Na_{sol}	20.48	2.63	2.26	5.55	2.55	2.40	0.76	0.58	0.58	-	-	-
Mg_{sol}	22.89	2.94	2.45	5.25	2.05	2.38	0.76	0.62	0.64	11	10	7
Zn_{sol}	309.59	7.54	3.15	0.17	0.76	0.48	0.84	0.66	0.65	93	65	28
Al_{sol}	56.98	5.38	2.79	2.45	1.56	0.58	0.81	0.68	0.63	64	51	19

Captions of Supplementary Electronic Materials

Fig. S1 Test solutions condition before the experiment

Fig. S2 Appearance of solutions and specimens after immersion in the solutions for 1, 2 and 3 d at 25, 50 and 80°C.

Fig. S3 Appearance of specimen surface after immersion in the solutions for 3 d at 25, 50 and 80°C a) before ultrasonic cleaning, b) after ultrasonic cleaning.

Fig. S4 AFM 3D images of specimen surface after immersion in the solutions for 3 d at 25, 50 and 80°C.

Fig. S1 Test solutions condition before the experiment

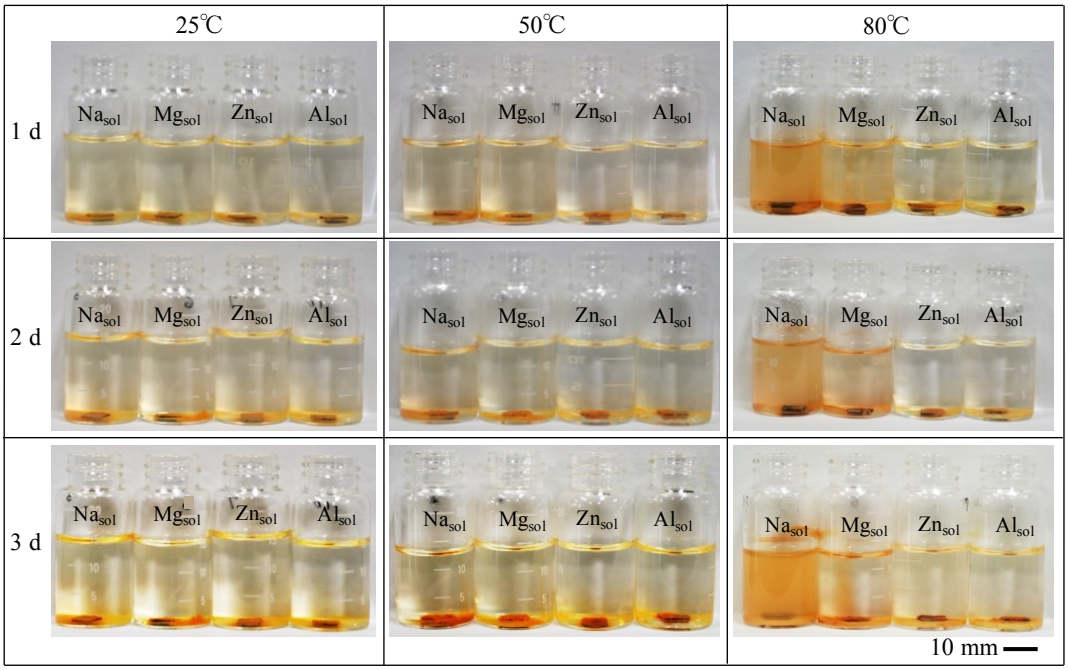

Fig. S2 Appearance of solutions and specimens after immersion in the solutions for 1, 2 and 3 d at 25, 50 and 80°C.

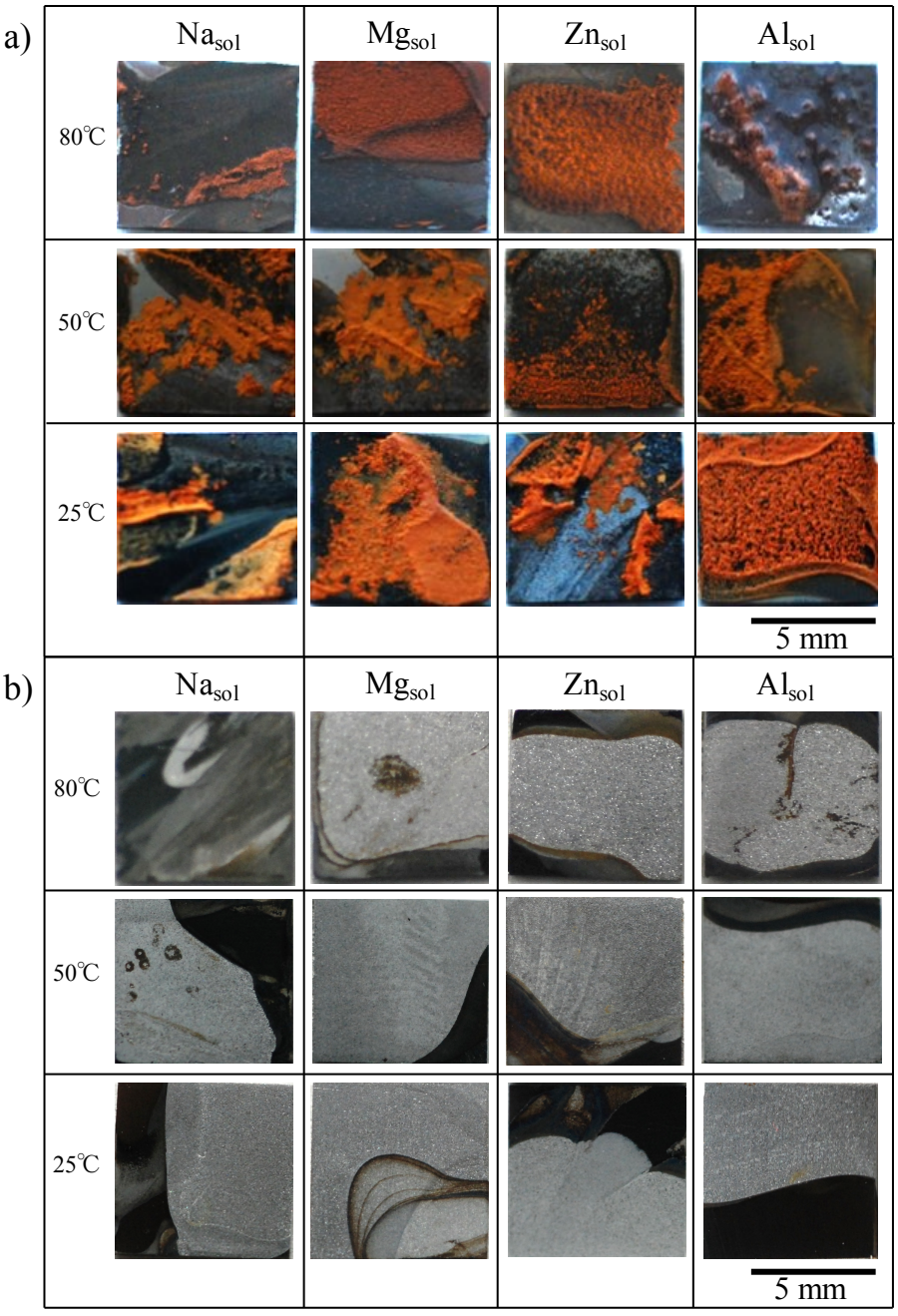

Fig. S3 Appearance of specimen surface after immersion in the solutions for 3 d at 25, 50 and 80°C a) before ultrasonic cleaning, b) after ultrasonic cleaning.

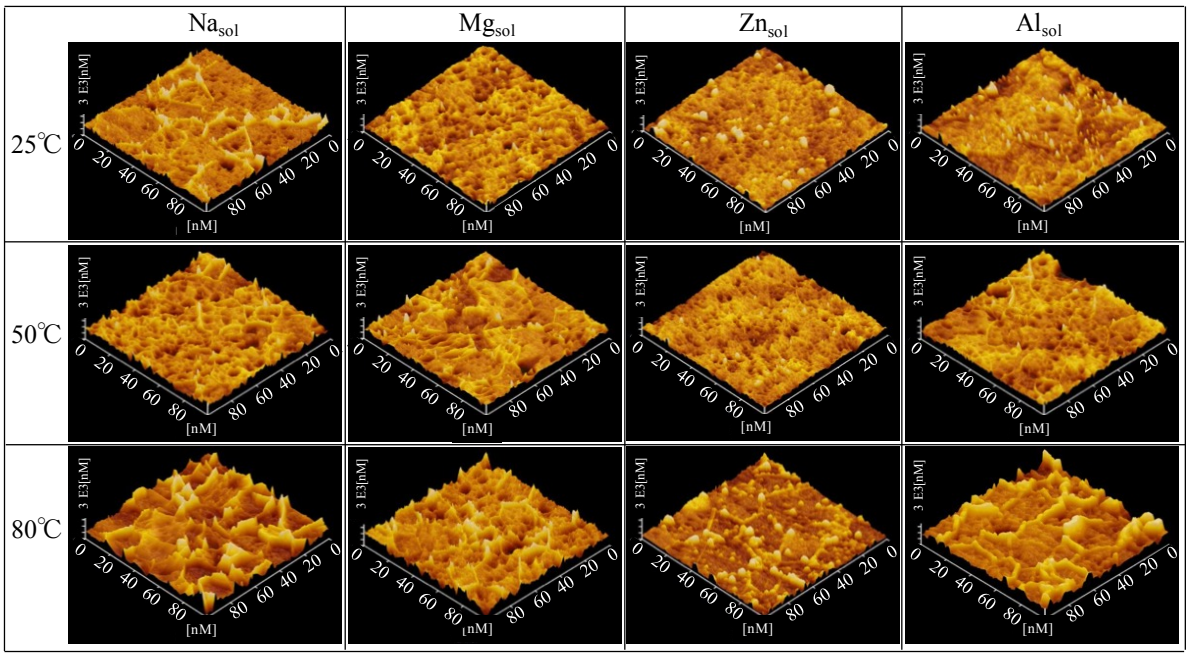

Fig. S4 AFM 3D images of specimen surface after immersion in the solutions for 3 d at 25, 50 and 80°C.

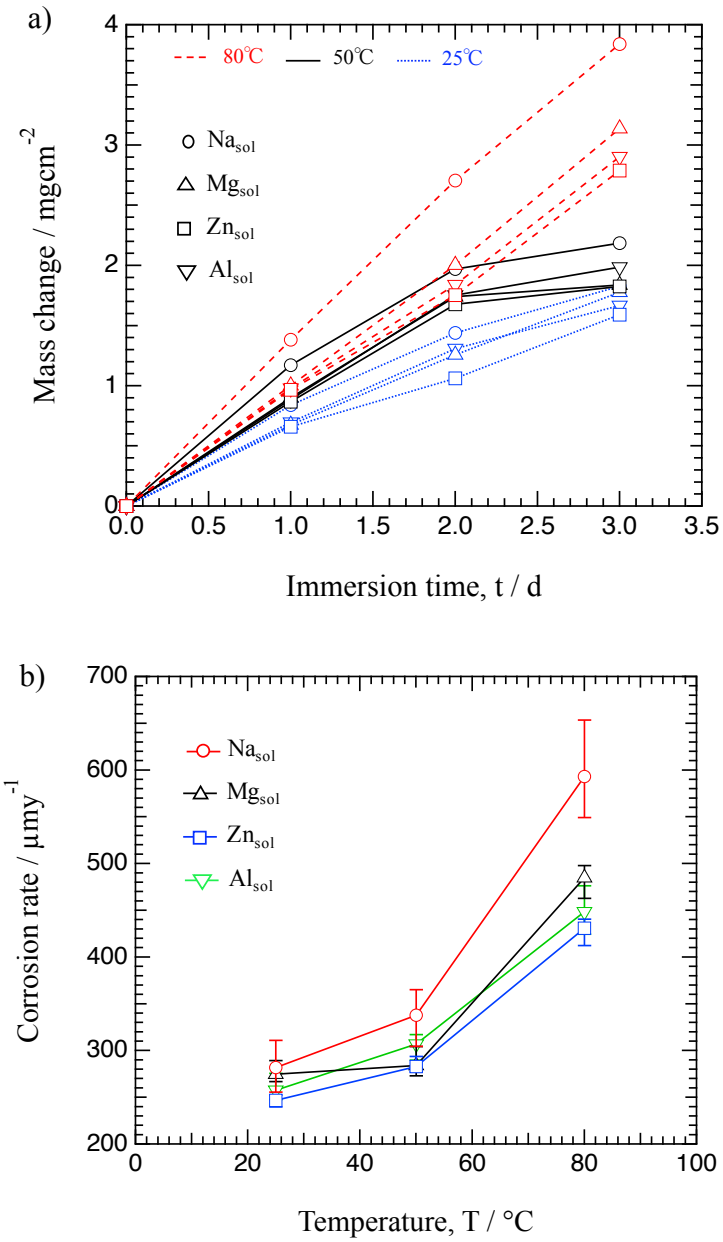

Fig. 1 a) Mass changes of specimens with immersion time and b) Corrosion rate at different temperatures.

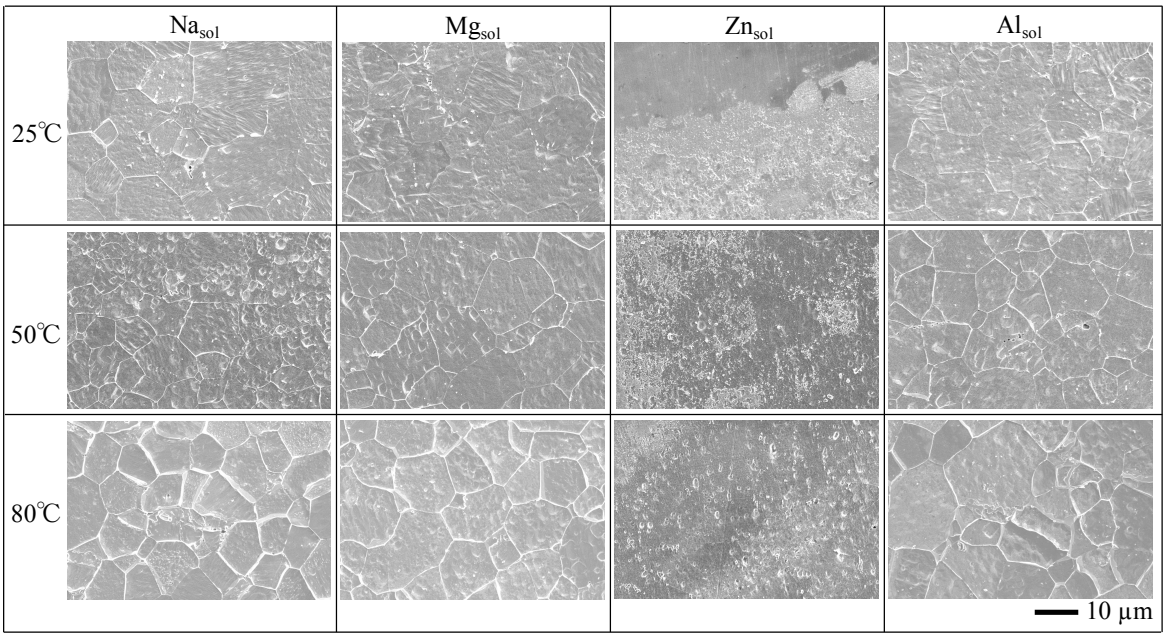

Fig. 2 Surface SEM images of specimen after immersion in the solutions for 3 d at 25, 50 and 80°C.

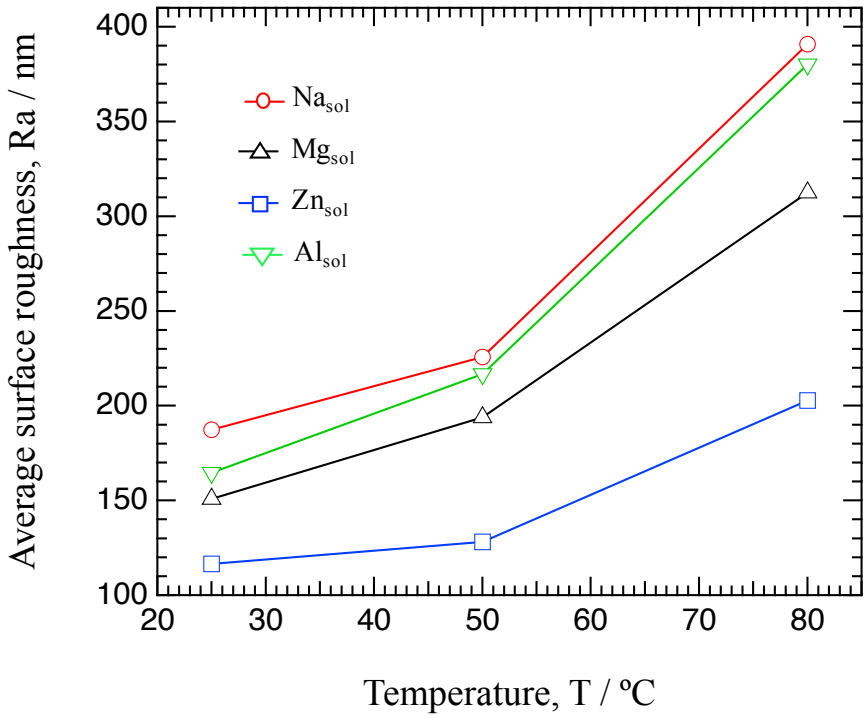

Fig. 3 Average surface roughness of specimens as a function of temperature after immersion in the solutions for 3 d.

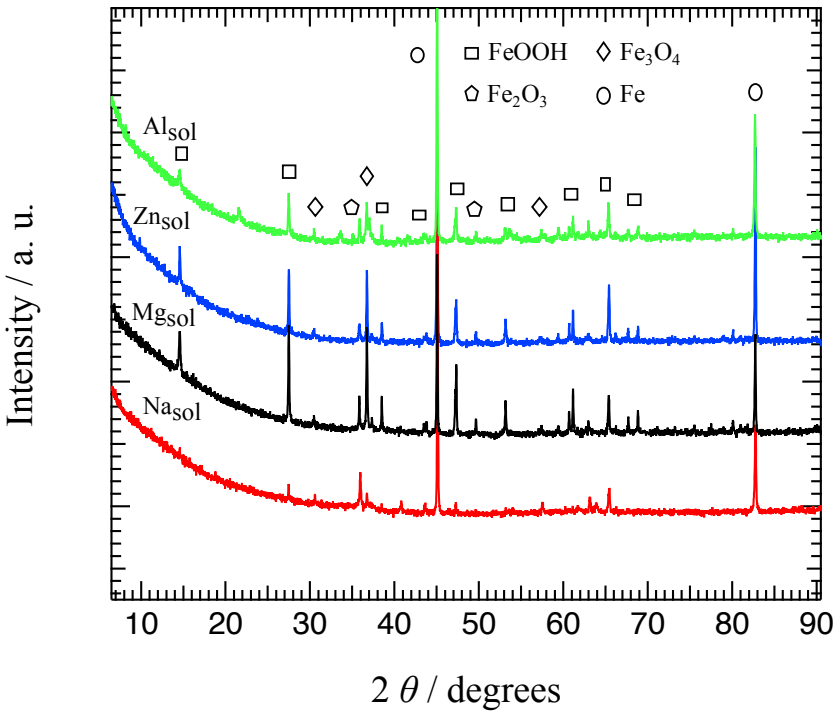

Fig. 4 XRD patterns of the corrosion products (rust) formed on specimens after immersion in the solutions for 3 d at 80°C.

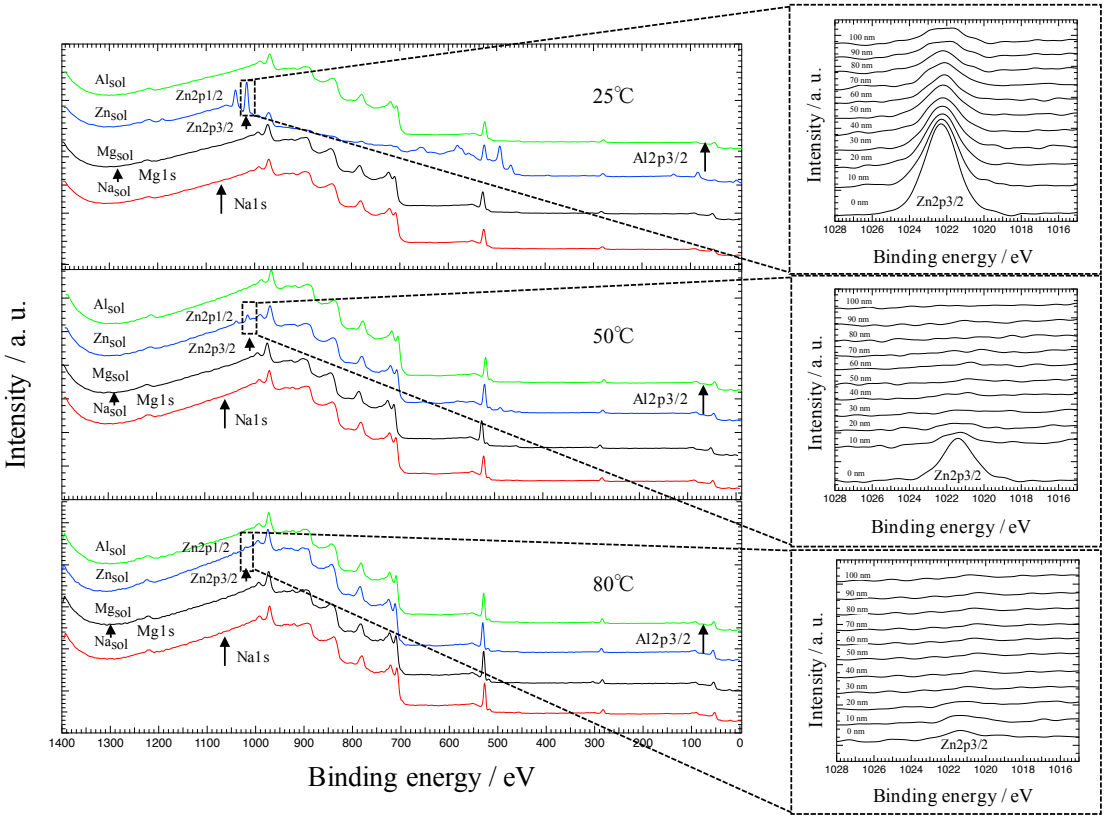

Fig. 5 XPS wide spectra of specimen surface after immersion in the solutions for 1 h and narrow spectra of Zn2p3/2 with depths (inset) at 25, 50 and 80°C.

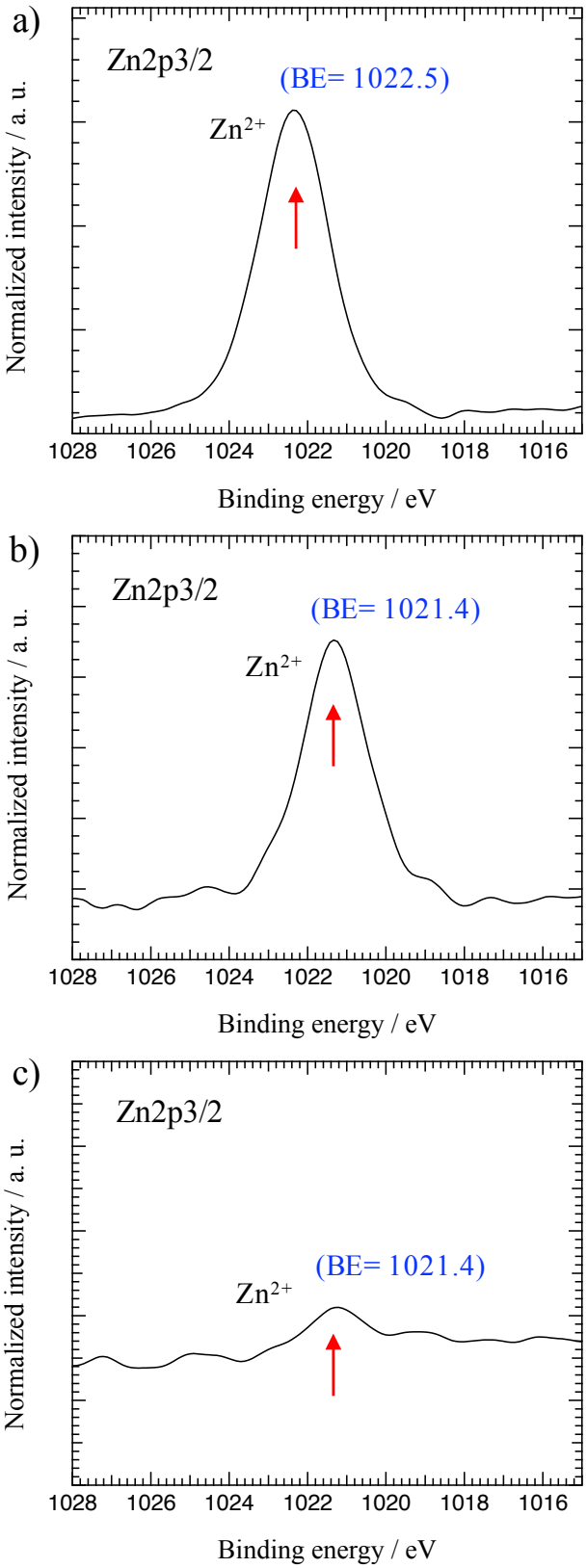

Fig. 6 XPS narrow spectra of Zn2p3/2 with chemical state and binding energy at a) 25°C, b) 50°C and c) 80°C.

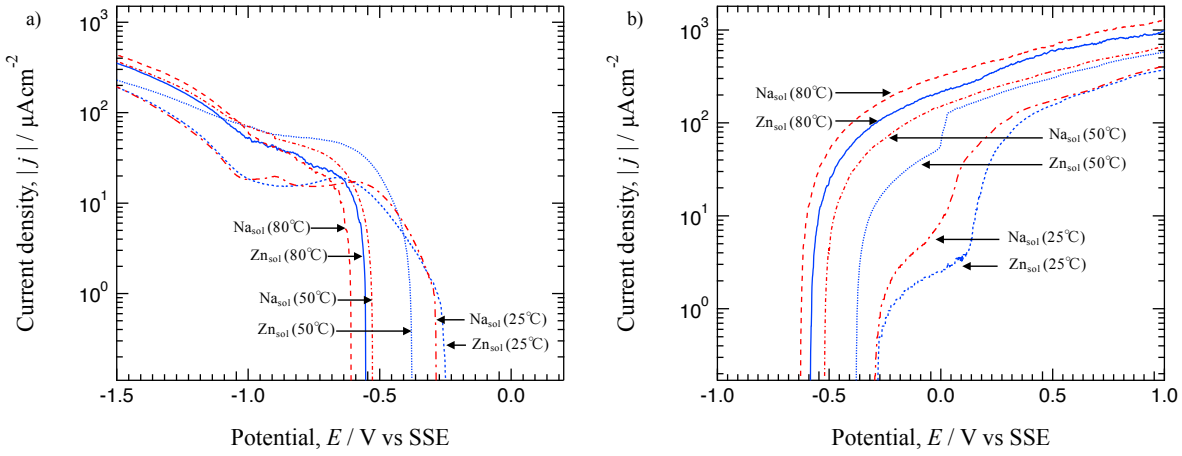

Fig. 7 Potentiodynamic a) cathodic and b) anodic polarization curves after immersion in the Na_{sol} and Zn_{sol} solutions for 1 h at 25, 50 and 80°C.

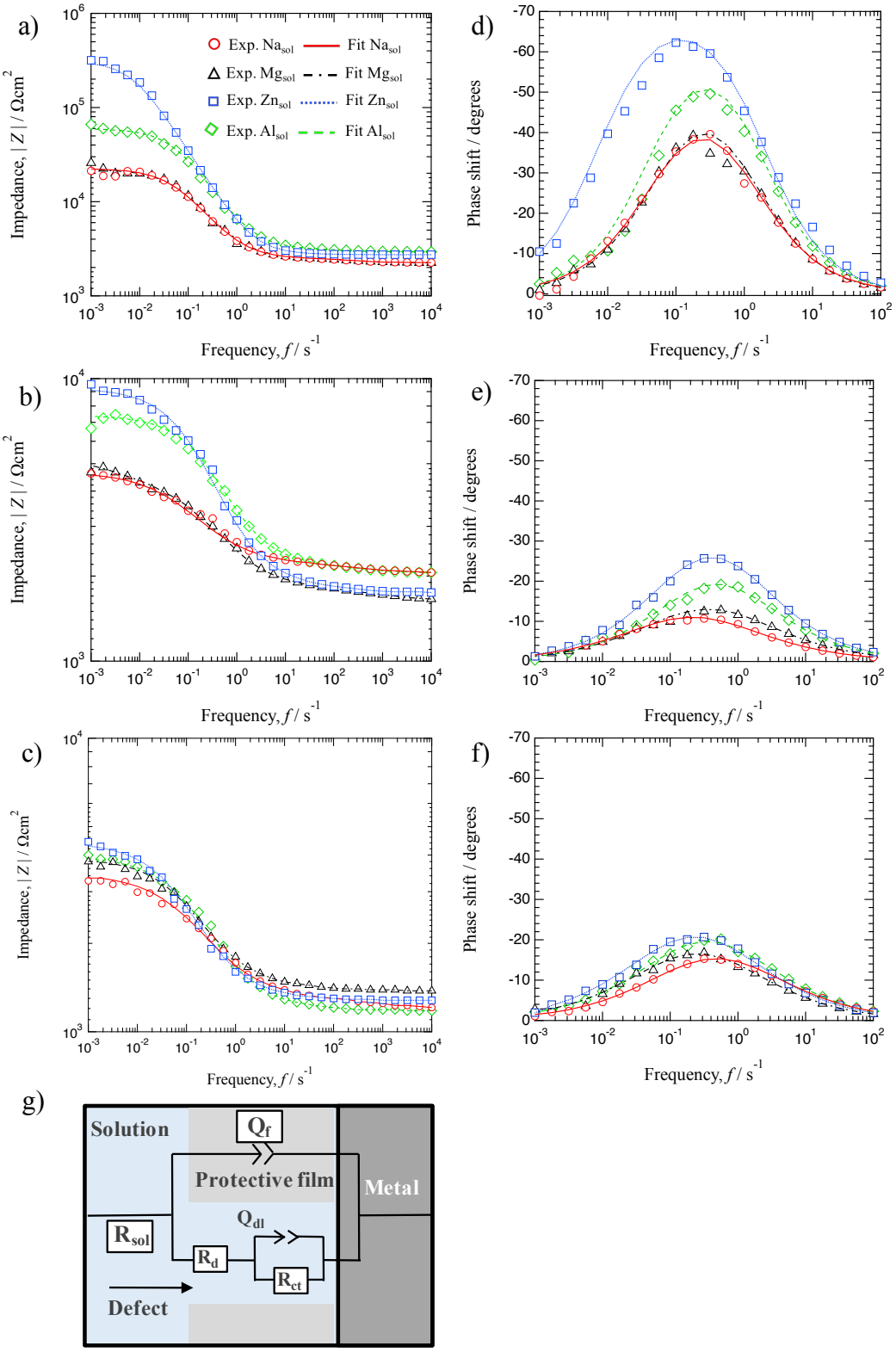

Fig. 8 Bode diagram of impedance and phase shift plots a) and d) at 25°C, b) and e) at 50°C, c) and f) at 80°C, and g) Schematic representation of equivalent circuit of mild steel electrode with a protective film having defect.

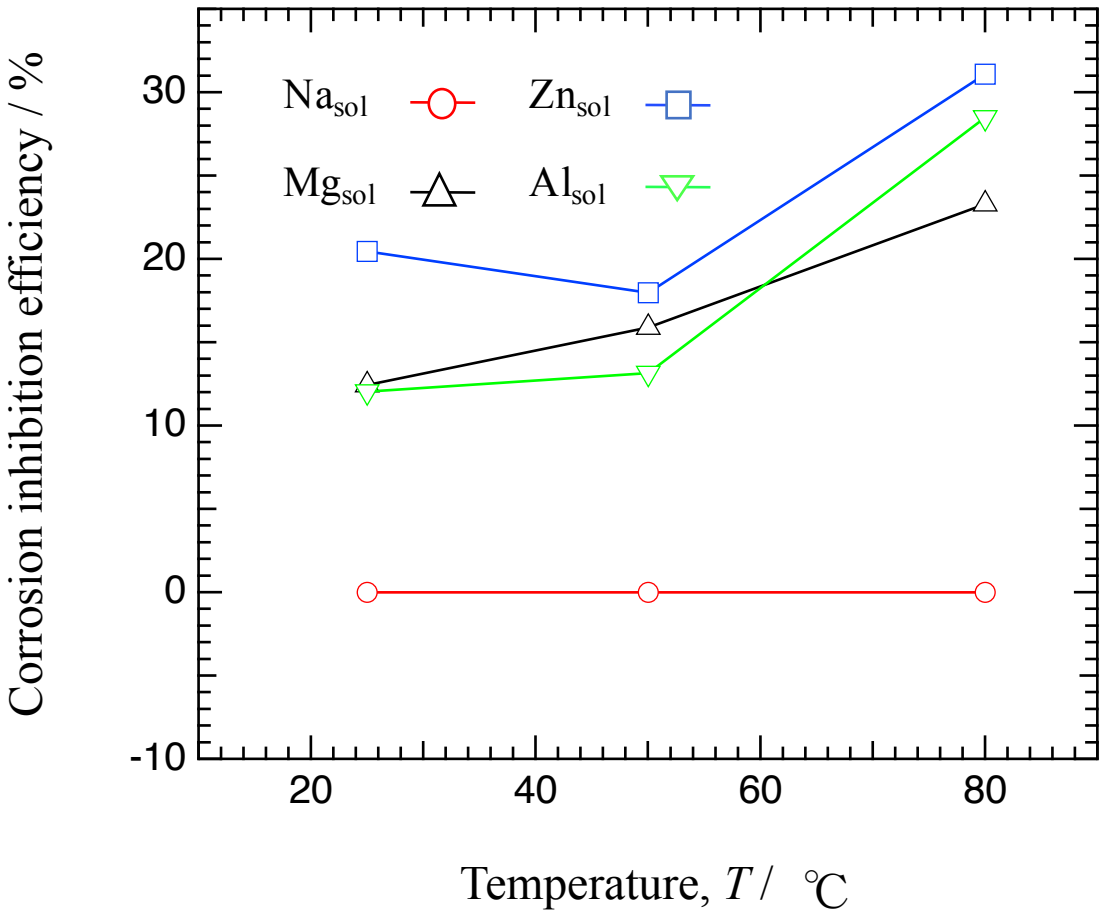

Fig. 9 Corrosion inhibition efficiency of metal cations as a function of temperature.

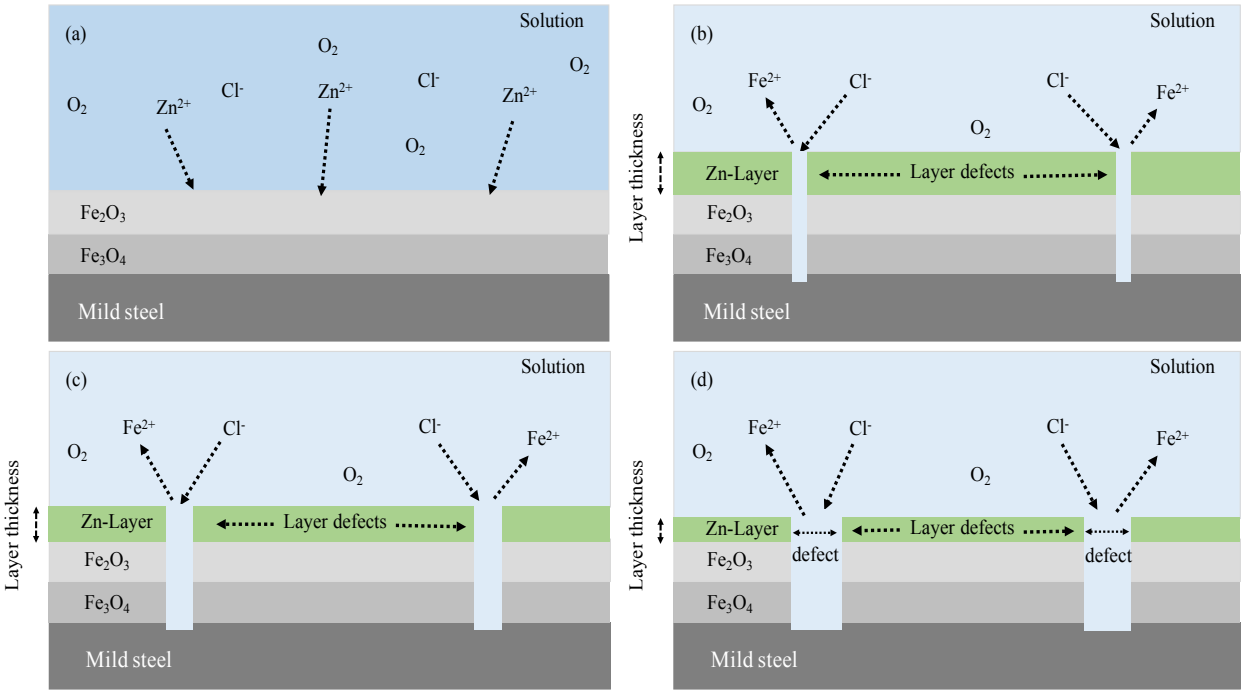

Fig. 10 Corrosion inhibition mechanism of mild steel by the Zn-layer at different temperatures, a) Formation of Zn-layer on the steel surface b) Cl^- attack at the defect sites and initiation of metal dissolution at 25°C c) Decreasing of Zn-layer thickness and increasing of defect area at 50°C d) Decreasing of Zn-layer thickness and increasing of defect area at 80°C.